A shear strength criterion for the buckling analysis of CLT walls

Olivier Perret, Cyril Douthe, Arthur Lebée, Karam Sab

▶ **To cite this version:**

Olivier Perret, Cyril Douthe, Arthur Lebée, Karam Sab. A shear strength criterion for the buckling analysis of CLT walls. Engineering Structures, 2020, 211, pp.110344. 10.1016/j.engstruct.2020.110344 . hal-02523678

HAL Id: hal-02523678

https://enpc.hal.science/hal-02523678v1

Submitted on 29 Mar 2020

HAL is a multi-disciplinary open access archive for the deposit and dissemination of scientific research documents, whether they are published or not. The documents may come from teaching and research institutions in France or abroad, or from public or private research centers.

L'archive ouverte pluridisciplinaire **HAL**, est destinée au dépôt et à la diffusion de documents scientifiques de niveau recherche, publiés ou non, émanant des établissements d'enseignement et de recherche français ou étrangers, des laboratoires publics ou privés.

A shear strength criterion for the buckling analysis of CLT walls

Olivier Perret[a], Cyril Douthe[a,*], Arthur Lebee[a], Karam Sab[a]

[a]*Laboratoire Navier, UMR 8205, École des Ponts ParisTech, IFSTTAR, CNRS, Champs-sur-Marne, France*

Abstract

The proper sizing of Cross Laminated Timber (CLT) walls for the construction of high rise buildings requires to take into account their low shear stiffness and their viscoelastic properties and to integrate them into the framework of actual building codes which are all based upon Ayrton-Perry approach of imperfect columns. The present paper starts thus by recalling the framework of Linear Buckling Analysis of shear weak columns using the Timoshenko beam model. Then, Ayrton-Perry approach of the buckling of imperfect columns is introduced and used to develop a normal stress strength criterion for CLT walls but also an additional shear strength criterion. Both criteria are compared for three characteristic sizes of initial imperfections. Afterwards, orthotropic creep is introduced and its effect on long term stability of shear weak members is investigated and an extension of the previous criteria to long term behaviour is developed. Throughout the study, three numerical examples are used for illustration (a low strength panel, a high strength and an aerated panel) revealing the importance of proposed shear strength verification and the need of experimental characterisation.

Keywords: Ayrton-Perry, shear weak members, rolling shear, creep buckling, geometric imperfection.

1. Introduction

1.1. About CLT walls

Cross Laminated Timber (CLT) walls belongs to the category of shear-weak columns. The literature on the subject is abundant: a chapter with an extended bibliography is dedicated to them in Bazant [1] for instance. In the steel construction industry, built-up columns are a wellknown case of such columns where taking the shear stiffness is mandatory (see for example [2, 3]), while in the aeronautic industry, one might think to sandwich panels under compression [4, 5, 6]. The particularities of CLT walls lay mainly in their heterogeneities (at board scale and layer scale) and also in their viscoelastic behaviour at long term. The proper sizing of CLT walls for the construction of high rise buildings will thus require to take into account these properties and to integrate them into the framework of actual building codes which are all built around Ayrton-Perry's approach of imperfect columns [7].

*Corresponding author

Email address: cyril.douthe@ifsttar.fr (Cyril Douthe)

1.2. On the buckling of imperfect column

In previous work [8], the authors investigated the linear buckling of CLT walls using several plate models, and provided there a thorough literature review on plate linear buckling which is not recalled here for conciseness. CLT walls were assumed perfectly straight, under a perfectly centered compressive load and simply supported on their four edges. Nonetheless, in actual structures, these assumptions may not always hold, for four reasons:

- First, CLT panels are not perfectly straight. There is no standard value for this out-of straightness but one might find indications in the literature. In the Eurocode 5 [9] for instance, a maximum initial straightness imperfection of 1/500 of the span is recommended for Laminated Veneer Lumber (LVL) and Glued Laminated Timber and of 1/300 of the span for solid timber. In the CLT Handbook [10], it is suggested that the deviation of edges from the straight line between two corners must not exceed 1.6 mm for CLT which corresponds to 1/2000 of the length for a 3-meters high wall.

- Second, the compression load is never perfectly centered. In its guide for application, the company Stora Enso [11] assumed that an eccentricity of the load equal to one sixth of the thickness of the CLT should be considered. This corresponds to 1/180 of the length for a slenderness of 30, which is quite important in comparison with out-of straightness imperfections.

- Third, inner stresses are locked in the panels. Indeed due to the crossing of the layers, deformations due to humidity are prevented which results in a set of self equilibrated inner stresses.

- Fourth, the boundary conditions of CLT walls are often realised through steel connectors that provide some lateral out-of-plane stiffness which might be one or two order of magnitude lower than the stiffness of the loaded edges.

To the authors knowledge, the buckling of a column with initial imperfections was first studied by Ayrton and Perry [12], at least in the realm of modern strength of materials. They analysed that all kinds of initial imperfections (geometric, material or loading imperfections) lead to additional bending moments, which induce an additional pre-buckling deflection. They then expressed this deflection as a function of the compressive load and formulated a strength criterion based on actual stresses in the deformed configuration. This strength criterion is known as Ayrton-Perry formula and is the reference for many modern standards. For instance, the design criterion of timber columns in the Eurocode 5 [9] is based on this formula. The kinematic model used is Euler's beam model, and therefore, it does not take shear stiffness into account. An extension of Ayrton-Perry approach to CLT walls was thus proposed by Thiel *et al* [7], using Timoshenko kinematics.

This new formula approaches better pre-buckling deformations and their influence on the critical buckling load which is still expressed as a strength criterion on longitudinal stresses. However, due to pre-buckling deformations, compression is deviated and goes with shear forces. In CLT panels, shear forces are resisted by rolling shear in cross-layers (i.e. shear in the radial/tangential plane), contrary to other timber products such as Glued Laminated Timber (GLT) or Laminated Veneer

Lumber (LVL). The rolling shear strength is however very low and much lower than longitudinal shear strength. One may thus ask if, in this case, the critical buckling load could correspond to a failure occuring in cross-layers due to excessive shear. The derivation of a shear criterion similar to Ayrton-Perry formula is thus the main goal of this paper.

1.3. On the influence of creep

Nonetheless, it is well known that wood creeps and that taking creep deformations into account is mandatory to properly design wood products. As part of the compressive forces in CLT walls are permanent forces, a panel under compression will thus creep and pre-buckling deformations will increase with time, which will lower the buckling load through time.

From Standards point of view [9], creep deformations after 50 years are taken into account through the creep factor k_{def} which depends on the service class: k_{def} is equal to 0.8 in service class 1 where moisture content is lower than 13%, and to 1.0 in service class 2 where moisture content is between 13% and 20% for solid timber (actual values for CLT are taken from oral communication of one member of the local CEN working group) . Currently, in the Eurocode 5 [9], there is thus only one creep parameter which is fully in accordance with the fact that the reference beam model for calculations is always based on Euler kinematics. Yet, most recent studies on CLT panels [8, 13, 14] tend to demonstrate that taking shear stiffness into account is relevant for CLT, which consequently implies the identification of orthotropic creep factors based on long term mechanical properties in the various layers.

Therefore, one often relies on test at ring scale. For example, tensile and shear creep tests in all directions were conducted by Schniewind *et al.* on Douglas fir [15]. First, they observed that creep in radial R and tangential T directions is almost 8 times larger than creep in longitudinal direction after 1000 minutes corresponding to the primary creep. Second, they observed that the shear creep in the longitudinal-tangential plane is between 4 to 5 times larger than the longitudinal tensile creep. From these observations, they concluded that each parameter should be considered individually.

Considering sollicitations in CLT panels, at least two additional parameters must be included in calculations: the longitudinal-radial shear stiffness G_{LC} and the cross-layer shear stiffness G_{CZ}. Only few studies on the creep behavior of CLT have been conducted [16, 17, 18]. Jobst *et al* [16] compared the creep behavior of glue-laminated timber (GLT) and of CLT from four-point bending tests during one year. They observed that the relative creep of 5-ply CLT is 39% to 47% higher than GLT. From their tests, they then calculate the shear creep of the cross-layer in order to extend their results to all CLT configurations. Their interpretation is however questionnable as the proper identification of the shear stiffness at layer scale is still under debate because its indirect measurement is extremely sensitive to the accuracy of the bending stiffness estimation in CLT panels [19, 20]. Consequently, additional experimental data seems necessary to characterize directly the longitudinal-layer shear creep factor $k_{\text{def},0-90}$ and the cross-layer shear creep factor $k_{\text{def},90-90}$.

Hence, despite the lack of experimental data, it appears that an appropriate criterion for long term buckling of CLT panels should be able to differentiate the effect of shear creep from longitudinal creep. The introduction of both effects into the afore mentionned Ayrton-Perry approach is the second objective of this paper.

1.4. Contribution

The present paper will thus be organised as follow. In Section 2, the framework of Linear Buckling Analysis of shear weak columns will be recalled using the Timoshenko beam model with practical applications to CLT walls. Then, in Section 3, Ayrton-Perry approach of the buckling of imperfect columns will be introduced and used to develop a normal stress strength criterion and also a new shear strength criterion. Both criteria will be compared for three typical configurations of CLT and for three characteristic sizes of initial imperfections. Afterwards, orthotropic creep will be introduced and its effect on long term stability of shear weak members will be investigated in Section 4. Throughout the study, three numerical examples will be used for illustration: one low strength panel, one high strength and one aerated panel. A comparison with EC5 is finally discussed in the conclusion.

2. Linear buckling analysis of shear weak columns

2.1. Linear buckling of columns without imperfections

The framework of the present derivation is similar to that of Bazant [1] (*chapter 11.6 Column or plate with shear: finite strain effects*). CLT walls are considered as simply supported rectangular column with a length l, a width b and a thickness h corresponding to the x, y and z directions respectively (Figure 1). Typical dimensions are the following: $l \approx 3\,\text{m}$, $b \approx 6\,\text{m}$ and $h \approx 0.2\,\text{m}$. The width b being much larger than the thickness h, only buckling in the z direction is investigated in the following. The cross section is supposed homogeneous in the x and y direction and heterogeneous through the thickness h in the z direction to account for variations of the layer orientation through the thickness of the CLT panel. The Young modulus in x direction is noted $E_0(z)$ and the shear modulus between x and z direction $G_0(z)$. These material characteristics are assumed to vary with z.

In the Timoshenko beam model for shear weak members, the 3D displacement field $\underline{\boldsymbol{u}}(x, y, z)$ is a function of the deflection of the beam neutral axis $f(x)$ and of the rotation of the section $\varphi(x)$:

$$\begin{cases} u_x(x, y, z) = \varphi(x) z & \text{(1a)} \\ u_y(x, y, z) = 0 & \text{(1b)} \\ u_z(x, y, z) = f(x) & \text{(1c)} \end{cases}$$

The generalized shear strain $\gamma(x)$ complies then with the compatibility equation:

$$\gamma(x) = \varphi(x) + f'(x) \tag{2}$$

where $\bullet' = \frac{d\bullet}{dx}$ stands for the first derivative of the function $\bullet$ with respect to x.

The axial stiffness $\overline{ES_0}$, the bending stiffness $\overline{EI_0}$ and the shear stiffness $\overline{GS_0}$ of the beam are

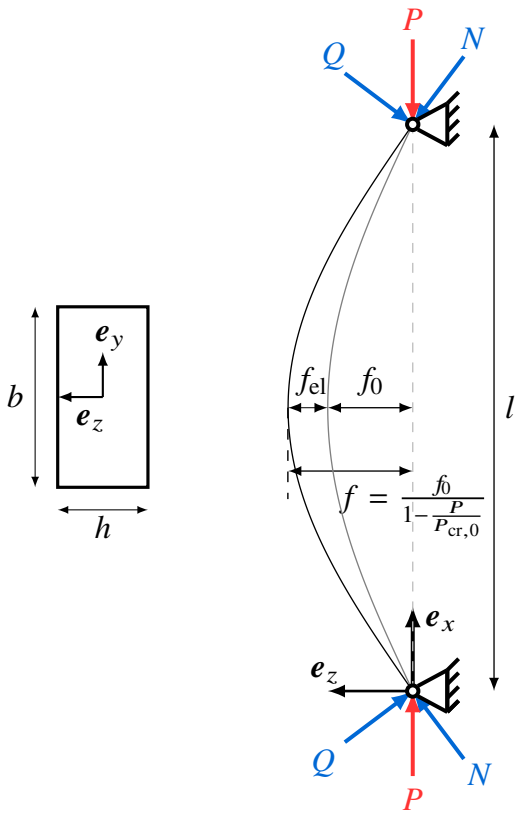

Figure 1: Scheme of the reference beam configuration under compression load with and without initial imperfection, and deformed configuration.

derived classically from Timoshenko's beam model and Jourawski's hypothesis for shear stresses:

$$\begin{cases} \overline{ES}_0 = \displaystyle\int_{-\frac{h}{2}}^{\frac{h}{2}} bE_0(z)dz & \text{(3a)} \\ \overline{EI}_0 = \displaystyle\int_{-\frac{h}{2}}^{\frac{h}{2}} bz^2E_0(z)dz & \text{(3b)} \\ \dfrac{1}{\overline{GS}_0} = \dfrac{b}{\overline{EI}_0^2}\displaystyle\int_{-\frac{h}{2}}^{\frac{h}{2}} \left(\int_{-\frac{h}{2}}^{z} E_0(t)tdt\right)^2 \frac{1}{G_0(z)}dz & \text{(3c)} \end{cases}$$

The bending moment $M(x)$ and the shear force $Q(x)$ are related to the deformations by the usual constitutive relations:

$$\begin{cases} M(x) = \overline{EI}_0\varphi'(x) & \text{(4a)} \\ Q(x) = \overline{GS}_0\gamma(x) & \text{(4b)} \end{cases}$$

Considering then the static equilibrium of a small section of columns under the centered compression load P in the deformed configuration:

$$\begin{cases} Q = M' & \text{(5a)} \\ M - Pf = 0 & \text{(5b)} \end{cases}$$

and introducing the behaviour (4), the typical equations of linear buckling analysis are retrieved:

$$\begin{cases} f'' + K_T^2 f = 0 & \text{(6a)} \\ \varphi'' + K_T^2\varphi = 0 & \text{(6b)} \end{cases}$$

where K_T can be seen as a correction of Euler-Bernouilli K_E which takes the shear compliance $\overline{GS_0}$ into account:

$$K_T^2 = K_E^2 \frac{1}{1 - \frac{P}{\overline{GS_0}}} \qquad \text{and} \qquad K_E^2 = \frac{P}{\overline{EI_0}}. \tag{7}$$

Considering then simply supported boundary conditions:

$$f(0) = f(l) = 0 \qquad \text{and} \qquad \varphi'(0) = \varphi'(l) = 0,$$

non-trivial solutions of the eigenvalue problem (6) can be easily found in the form of a sine function with undetermined amplitude A:

$$f(x) = A \sin(K_T x) \qquad \text{and} \qquad \varphi(x) = -AK_T \cos(K_T x) \tag{8}$$

Hence, it appears that the first critical buckling load $P_{\text{cr},0}$ is given by:

$$\frac{1}{P_{\text{cr},0}} = \frac{1}{P_{E,0}} + \frac{1}{\overline{GS_0}} \quad \text{where} \quad P_{E,0} = \overline{EI_0} \frac{\pi^2}{l^2} \tag{9}$$

$P_{E,0}$ is the first Euler critical buckling load associated to the Euler beam theory where a zero shear compliance $\frac{1}{\overline{GS_0}}$ is assumed. It is remarked in equation(9) that the contribution of the shear stiffness $\overline{GS_0}$ does not depend on the mode, so that the higher the mode, the higher the influence of the shear stiffness on the corresponding buckling load.

At bifurcation, the shear deformation and rotation of the beam neutral axis are finally given by:

$$\varphi(x) = -\frac{P_{\text{cr},0}}{P_{E,0}} \frac{\pi}{l} A \cos \frac{\pi x}{l} \quad \text{and} \quad \gamma(x) = \frac{P_{\text{cr},0}}{\overline{GS_0}} \frac{\pi}{l} A \cos \frac{\pi x}{l} \tag{10}$$

The local normal stresses $\sigma = \sigma_{xx}$ and shear stresses $\tau = \sigma_{xz}$ in the layers are then computed from the beam forces and the local material properties by:

$$\begin{cases} \sigma(x,z) = -\dfrac{P}{\overline{ES_0}} E_0(z) + \dfrac{zM(x)}{\overline{EI_0}} E_0(z) & \text{(11a)} \\ \tau(x,z) = \dfrac{Q(x)}{\overline{EI_0}} \displaystyle\int_z^{\frac{h}{2}} E_0(z) z dz & \text{(11b)} \end{cases}$$

Then, introducing the global behaviour (4) and the shape of the first buckling mode (10), leads to the stress state at bifurcation (i.e. for $P = P_{\text{cr},0}$):

$$\begin{cases} \sigma(x,z) = -\dfrac{P_{\text{cr},0}}{\overline{ES_0}} E_0(z) - zE_0(z) \dfrac{P_{\text{cr},0}}{P_{E,0}} \dfrac{\pi^2}{l^2} A \sin \dfrac{\pi x}{l} & \text{(12a)} \\ \tau(x,z) = \dfrac{P_{\text{cr},0}}{\overline{EI_0}} \dfrac{\pi}{l} A \cos \dfrac{\pi x}{l} \displaystyle\int_z^{h/2} E_0(z) z dz & \text{(12b)} \end{cases}$$

Rupture will occur when one of these stresses reaches the corresponding limit strength. Considering the distribution of compression stresses in (12), it appears that the maximum compression stress is

reached at $x = l/2$ and $z = -h/2$, which corresponds to a longitudinal layer where $E_0(h/2) = E_L$. In the same way, the maximum shear stress is reached in $x = 0$ and $z = 0$. The orientation of the middle layer depends however on the structure of the panel (see Figure 2). Considering the relative order of magnitude of the rolling shear strength and the longitudinal shear strength, it appears clearly that rupture will occur in the most central cross layer (in which shear forces are in the radial tangential plane). Considering also that the shear stresses in (12) vary slowly around $z = 0$, it will be conservatively assumed in the following that the maximum rolling shear stress is obtained for $z = 0$. Hence, the extreme values of compressive and rolling shear stress are proportionnal to the amplitude of the buckling mode:

$$\begin{cases} \sigma\left(\frac{l}{2}, \frac{-h}{2}\right) = -\frac{P_{\text{cr},0}}{\overline{ES}_0} E_L - A\frac{h}{2} E_L \frac{P_{\text{cr},0}}{P_{E,0}} \frac{\pi^2}{l^2} = \sigma_N + A\sigma_M & \text{(13a)} \\ \tau(0,0) = A\frac{P_{\text{cr},0}}{\overline{EI}_0} \frac{\pi}{l} \int_0^{h/2} E_0(z) z dz = A\tau_{\max} & \text{(13b)} \end{cases}$$

2.2. *Influence of the shear stiffness on the buckling load*

We will now illustrate the influence of shear stiffness $\overline{GS}_0$ on the critical buckling load by investigating three realistic configurations of CLT walls (see Table 1).

- CLT1 represents a slender high strength panel, it is a 3-ply standard CLT ($40 - 40^T - 40$) of class CL32h made of boards with an $\frac{w_p}{t_p}$ smaller than 4 and thus an equivalent cross-layer rolling shear stiffness of $G_{CZ} = 65\,\text{MPa}$ and rolling shear strength of $\tau_u = 0.8\,\text{MPa}$ [19, 20, 21, 22, 23].

- CLT2 is a thick 7-ply panel ($80 - 40^T - 40 - 40^T - 80$) of standard CL24h class for which the aspect ratio of boards $\frac{w_p}{t_p}$ is again smaller than 4, which induces a reduced rolling shear stiffness $G_{CZ} = 65\,\text{MPa}$ and a reduced rolling shear strength $\tau_u = 0.8\,\text{MPa}$.

- CLT3 is an aerated CLT with a similar configuration to CLT2 ($80 - 40^T - 40 - 40^T - 80$), but with 50% of voids in the three central layers. (This kind of configuration becomes indeed more and more popular in the last decade [24, 25, 26]. Similar local properties will be considered as CLT2 except for the rolling shear strength for which an equivalent strength of $\alpha_p^2 \tau_u$ is chosen because the contact between the central layer is ensured by one fourth (α_p^2) of the total surface, so that the maximum stress is four times the average evaluated by expression (13b).

For the mean longitudinal shear modulus, CLT panels without narrow face boundings are considered, so that according to [22, 23], $G_{LC} = 450\,\text{MPa}$. The three configurations are hence summarized in Figure 2 and their characteristics are recalled in Table 1. The local axes used for the definition of material properties are defined according to the fibre orientation and considering an averaging of property in the radial/tangential plane as illustrated in Figure 3 (see also [23] for the evaluation of close form average properties).

For each configuration, equivalent beam/plate stiffnesses are evaluated from (3a, 3b, 3c) which are evaluated hereafter for a multilayer panel. We note t_p the thickness of layer p, z_p the height of

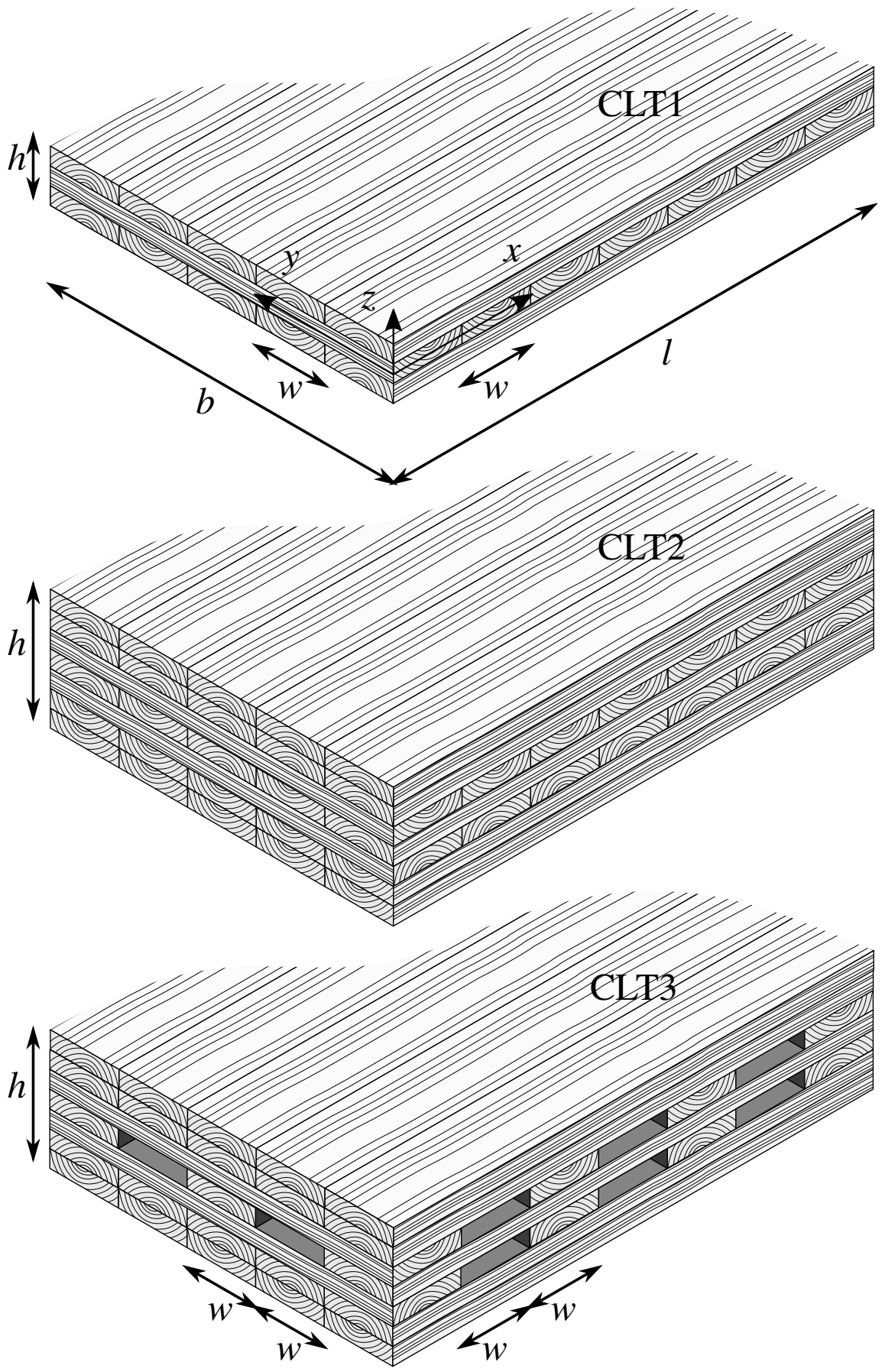

Figure 2: Three reference configurations of CLT: low strength, high strength and aerated.

	config	class	E_L	G_{LC}	E_C	G_{CZ}	σ_u	τ_u
CLT1	40-40^T-40	CL32h	12,500	450	300	65	32	0.8
CLT2	80-40^T-40-40^T-80	CL24h	11,500	450	300	65	24	0.8
CLT3	80-40^T-40-40^T-80	aerated	11,500	450	300	65	24	0.2

Table 1: Characteristics of the three CLT configurations (all values in MPa).

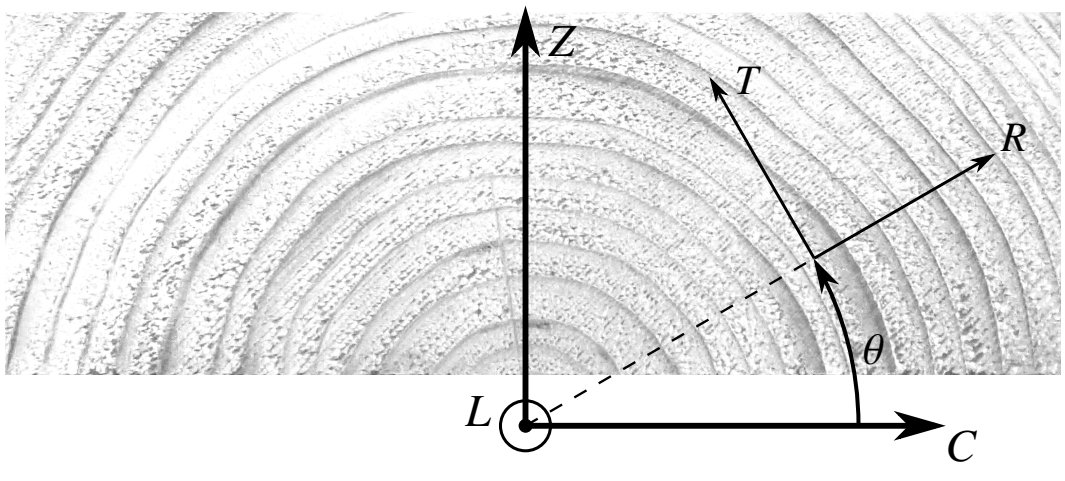

Figure 3: Local axes considered for each layer of the CLT panel.

its middle plane, E_p and G_p the Young and shear modulii expressed in the direction depending on the layer orientation in the panel's main frame (x, y, z in Figure 2). We note also α_p the volume fraction of void in the layer, $\alpha_p = 1$ except for the three central layers of CLT3 where $\alpha_p = 0.5$. And hence, for a wall with a width b, the equivalent beam stiffness are given by:

$$\begin{cases} \overline{ES}_0 = b \sum_{p=1}^{n} \alpha_p E_p t_p & \text{(14a)} \\ \overline{EI}_0 = b \sum_{p=1}^{n} \alpha_p E_p t_p \left(z_p^2 + \frac{t_p^2}{12} \right) & \text{(14b)} \\ \frac{1}{\overline{GS}_0} = \frac{1}{b} \frac{1}{\overline{EI}_0^2} \sum_{p=1}^{n} \frac{1}{\alpha_p G_p} \frac{t_p}{12} \left(12 g_p^2 + \left(z_p^2 + \frac{t_p^2}{60} \right) \alpha_p^2 E_p^2 t_p^2 \right) & \text{(14c)} \end{cases}$$

where the static momentum g_p in the middle of layer p is given by:

$$g_p = \sum_{q=1}^{p} \alpha_q E_q t_q z_q - \frac{1}{2} \left(z_p + \frac{t_p}{6} \right) \alpha_p E_p t_p \qquad \text{(15)}$$

Note that Franzoni *et al* have shown that for aerated CLT, this approach overstimates $\overline{GS}_0$ and that structure effects must also be taken into account in the estimation of the equivalent shear stiffness [24, 25].

The resulting stiffnesses are shown in Table 2 and the critical buckling loads for a 2.72 m high wall are shown in Table 3. In the three configurations, the shear stiffness $\overline{GS}_0$ is very low compared to the normal stiffness $\overline{ES}_0$, and appears comparable in order of magnitude to the bending stiffness $\frac{\overline{EI}_0}{l^2}$ for CLT3. This induces a significant difference between Euler's critical load $P_{E,0}$ and Timoshenko's critical load $P_{\text{cr},0}$ which falls to 36% of $P_{E,0}$ for the aerated CLT. Considering shear stiffness in the evaluation of the the critical buckling load of CLT walls is thus mandatory as concluded by [13].

Calculating then the ratio between the maximum bending stress in the longitudinal layers σ_M (13a) and the maximum shear stress in the cross layers τ_{max} (13b) and comparing this ratio with the

Config.	$\overline{ES_0}$ [kN/m]	$\overline{EI_0}$ [kNm^2/m]	$\overline{GS_0}$ [kN/m]	$\frac{\overline{EI_0}}{l^2}$ [kN/m]
CLT1	1,010,000	2,000	14,500	270
CLT2	2,320,000	21,600	37,300	2,950
CLT3	2,080,000	21,500	16,300	2,900

Table 2: Equivalent homogeneous beam stiffnesses of the three CLT configurations.

Config.	$P_{E,0}$ [kN/m]	$P_{\text{cr},0}$ [kN/m]	$P_{\text{cr},0}/P_{E,0}$	$\sigma_M/\tau_{\max}$	σ_u/τ_u
CLT1	2,670	2,260	84%	32	40
CLT2	28,800	16,200	56%	15	30
CLT3	28,600	10,400	36%	7	120

Table 3: Critical buckling loads and strength ratios for $b = 1m$ and $l = 2.72m$.

ratio between the longitudinal bending strength σ_u and the rolling shear strength τ_u, it is possible to estimate the failure mode of CLT walls. Both ratios for the three configurations are shown in Table 3. A higher value of σ_u/τ_u than $\sigma_M/\tau_{\max}$ indicates that failure may occur because of excessive shear force during buckling. From this simple linear buckling analysis, it appears that for all confi-gurations there is a risk for shear failure prior to longitudinal bending failure during buckling. It seems thus necessary to introduce a design criterion for shear strength in addition to the usual Ayrton-Perry criterion for longitudinal stresses.

3. Strength criteria for shear weak columns

3.1. Buckling of shear weak columns with initial imperfections

The Ayrton-Perry approach for the buckling of imperfect column generally refers to [12] which consider a beam in which the initial geometry is stress free and defined by:

$$f_0(x) = f_0 \sin\left(\frac{\pi x}{l}\right). \tag{16}$$

This out-of straightness defect f_0 corresponds generally to an equivalent imperfection that incorporates the three main kinds of imperfections (out-of straightness, material heterogeneity and eccentricity of loading). For simplicity of calculations, it is supposed that the imperfection shape takes the form of the first buckling mode (Figure 1). The initial imperfection $f_0(x)$ is supposed small compared to the wall height l.

Note here that there may be also an initial rotation imperfection $\varphi_0(x)$, but that it would not have additional impact on the column equilibrium if its form follows that of the first buckling mode (indeed (10) shows that both imperfections are proportional). It is therefore neglected, so that the shear deformation turns finally to:

$$\gamma(x) = \varphi(x) + f_{\text{el}}(x) = \varphi(x) + f'(x) - f_0'(x) \tag{17}$$

where f_{el} is the elastic part of the transverse deflection defined by:

$$f_{\text{el}}(x) = f'(x) - f_0'(x) \tag{18}$$

By injecting this expression in the transverse equilibrium (5), a new differential equation is obtained:

$$f''(x) + K_T^2 f(x) + \frac{\pi^2}{l^2} \frac{f_0}{1 - \frac{P}{\overline{GS}_0}} \sin \frac{\pi x}{l} = 0 \tag{19}$$

Taking into account the boundary conditions $f(0) = f(l) = 0$, it is found that:

$$f(x) = \frac{f_0}{1 - \frac{P}{P_{\text{cr},0}}} \sin \frac{\pi x}{l} \tag{20}$$

Note that the deflection is finite if and only if $P < P_{\text{cr},0}$: the column is stable only if the compressive load P is lower than the critical buckling load $P_{\text{cr},0}$. The elastic part of the deflection is then given by:

$$f_{\text{el}} = \frac{P}{P_{\text{cr},0}} \frac{f_0}{1 - \frac{P}{P_{\text{cr},0}}} \sin \frac{\pi x}{l} \tag{21}$$

Finally, from the constitutive equations (4) and the equilibrium (5a,5b), the shear strain γ and rotation rate φ in the column are expressed as:

$$\begin{cases} \gamma(x) = \dfrac{\pi}{l} \dfrac{P}{\overline{GS}_0} \dfrac{f_0}{1 - \frac{P}{P_{\text{cr},0}}} \cos \dfrac{\pi x}{l} & \text{(22a)} \\ \varphi(x) = -\dfrac{\pi}{l} \dfrac{P}{P_{E,0}} \dfrac{f_0}{1 - \frac{P}{P_{\text{cr},0}}} \cos \dfrac{\pi x}{l} & \text{(22b)} \end{cases}$$

3.2. Definition of a normal strength criterion

The Ayrton-Perry strength criterion is built on the evaluation of the maximum value of the longitudinal stress $\sigma_{\max}$ from the global deformation of the imperfect geometry (22b) and local behaviour (11a) and comparing it to the ultimate compressive strength σ_u. The maximum normal stress is obtained at mid span where $M(x)$ is maximum and on the external layer for $z = -\frac{h}{2}$. At this position, $E_0(z)$ is the longitudinal Young modulus E_L, and hence:

$$\sigma_{\max} = \frac{P}{\overline{ES}_0} E_L + \frac{P}{\overline{EI}_0} \frac{f_0}{1 - \frac{P}{P_{\text{cr},0}}} \frac{h}{2} E_L \tag{23}$$

So that, introducing the ultimate compressive load P_u and the addimensionnal imperfection ω defined by:

$$P_u = \sigma_u \frac{\overline{ES}_0}{E_L} \qquad \text{and} \qquad \omega = \frac{\overline{ES}_0 h f_0}{2\overline{EI}_0} \tag{24}$$

the failure criterion can finally be written as:

$$\frac{\sigma_{\max}}{\sigma_u} = \frac{P}{P_u} \left(1 + \frac{1}{1 - \frac{P}{P_{\text{cr},0}}} \omega \right) < 1 \tag{25}$$

Developping equation (25), it appears that the strength criterion $\frac{\sigma_{\max}}{\sigma_u} < 1$ is expressed as a criterion on a second order polynomial equation in P:

$$P^2 - \left[(1+\omega)\, P_{\mathrm{cr},0} + P_u\right] P + P_u P_{\mathrm{cr},0} > 0 \tag{26}$$

The validity domain of P is the one which satisfies the above equation and contains 0, it thus corresponds to values of P which are lower than the smallest root of (26), which writes:

$$\frac{P}{P_u} < \frac{2}{\left(1+\omega+\bar{\lambda}^2\right) + \sqrt{\left(1+\omega+\bar{\lambda}^2\right)^2 - 4\bar{\lambda}^2}} = \chi_\sigma \tag{27}$$

where $\bar{\lambda}$ is the modified slenderness defined by:

$$\bar{\lambda} = \sqrt{\frac{P_u}{P_{\mathrm{cr},0}}} \tag{28}$$

and χ_σ is the normalized compressive limit according to the normal strength criterion.

Following Ayrton-Perry approach, we found a design criterion for normal stress in CLT panels with free edges under pure compression which is very similar to that found by Thiel *et al* [13]. The main differences are:

1. The reference critical load $P_{\mathrm{cr},0}$ given by (9) incorporates the effect of shear stiffness (as in [13]), whereas Eurocode only accounts for longitudinal stiffness.

2. The section characteristics $\overline{ES}_0$ (3a) and $\overline{EI}_0$ (3b) are weighted averages that take into account the heterogeneity of the layers in terms of geometry and elastic properties.

3. Imperfections ω are related to the modified slenderness but differ in the expression (here $\omega = \frac{\overline{ES}_0 h f_0}{2\overline{EI}_0}$ whereas in EC5 $\omega = \beta_c\left(\bar{\lambda} - 0.3\right)$ where β_c is a factor associated with the fabrication process of the wooden member).

4. The duration of the load is not taken into account in (27) while EC5 uses $f_{c,0,k}$ to calculate $\bar{\lambda}$ and $f_{c,0,d} = \frac{f_{c,0,k}\, k_{\mathrm{mod}}}{\gamma_M}$ to calculate the limit strength in P_u. The proposed expression is consistent with a short term loading at short term after the construction.

Furthermore it has been seen in the conclusion of Section 2 that in CLT panels under compression, failure might occur due to excessive shear stress in cross layers. The development of a similar criterion for shear stresses, as a complement to normal stress criterion accounted in the Standards, seems thus important for CLT and will be achieved in the following section.

3.3. Definition of a shear criterion

We assume here that the shear force failure and the compression failure are not interacting since bending and shear effects are elastically uncoupled in the Timoshenko beam model and since the compression failure and the shear failure occur at different locations. As detailed in Section 2, the maximum compression occurs at mid-span whereas the maximum shear occurs at support ends.

From the constitutive law (4b) and the expression of the shear rate in the imperfect beam (22a), the maximum shear force $Q_{\max}$ at support ends can be calculated by:

$$Q_{\max} = \frac{\pi}{l} \frac{P f_0}{1 - \frac{P}{P_{\mathrm{cr},0}}} \tag{29}$$

Following the same reasoning as in Section 2, the expression of the maximum shear stress $\tau_{\max}$ is given by:

$$\tau_{\max} = \frac{Q_{\max}}{\overline{EI}_0} \int_0^{\frac{h}{2}} E_0(z) z dz \tag{30}$$

One can remark that this expression can be evaluated directly considering the first order rotation of the section at the support in Figure 1.

Hence, the ultimate shear force Q_u can be defined by:

$$Q_u = \tau_u \frac{\overline{EI}_0}{\int_0^{\frac{h}{2}} E_0(z) z dz} \tag{31}$$

Using the values of $Q_{\max}$ (29) and Q_u (31), the shear criterion of CLT wall given by $Q_{\max} < Q_u$ rewrites:

$$\frac{P}{P_u} < \frac{1}{\frac{\pi f_0}{l} \frac{P_u}{Q_u} + \bar{\lambda}^2} = \chi_\tau \tag{32}$$

χ_τ is the normalised compressive limit according to the shear strength criterion. Formally, this shear strength criterion is very similar to the normal strength criterion. It is thus possible to compare them and to test whether or not rolling shear failure might occur before bending failure in CLT walls under compression. This is done in the next section for practical configurations of panels.

3.4. Comparison of normal and shear criteria

First of all, it is noticed in (27) and (32) that, when the imperfection is zero ($f_0 = 0$), both criteria are identical: $\chi_\sigma = \chi_\tau = \frac{1}{\bar{\lambda}^2}$. Without imperfection, both criteria reduce to the linear buckling theory of a Timoshenko column.

Then, to investigate the influence of the imperfection size for the three CLT configurations previously studied (see Table 1), two amplitudes of imperfection are introduced:

- $f_0 = \frac{l}{200}$ as recommended in the Eurocode 5;
- $f_0 = \frac{l}{100}$ which might correspond to a load eccentricity of $\frac{h}{6}$ for a slenderness $\frac{l}{h} \approx 20$ (which is here the case of CLT1).

Both criteria (27) and (32) as function of the reduced slenderness $\bar{\lambda}$ (28) are plotted for CLT1, CLT2 and CLT3 in Figures 4, 5 and 6 respectively. Perfect columns are plotted in orange, standard columns in blue and highly imperfect columns in gray. The normal stress criterion is represented by dots, the shear stress criterion by crosses. Note that the reduced slenderness $\bar{\lambda}$ is not a linear

function of the column height and that it depends on the CLT configuration and on the imperfection size. Note also that there is a maximum value for the critical buckling load when the shear stiffness is taken into account (10) and therefore, the reduced slenderness has a limit value which is not zero (more precisely $\bar{\lambda}_{min}$ is equal to 0.40 for CLT1, 0.36 for CLT2 and 0.52 for CLT3, the higher the shear stiffness, the lower the limit value). Typical order of magnitude of $\bar{\lambda}$ are given for the three configurations in Table 4.

h	CLT1	CLT2	CLT3
3 m	1.09	0.58	0.67
6 m	2.07	0.97	1.00

Table 4: Order of magnitude of the modified slenderness $\bar{\lambda}$ at short term for the three reference configurations.

As expected, it is first remarked that the shear criteria are above the normal strength criteria for CLT1 and CLT2 but well below for CLT3: in aerated configurations the shear strength is the weak point and should be checked systematically (which is in accordance with all recommendations in the literature on the bending of such panels [24, 25]). Considering a panel with 2.72 m as in the previous section, the ratio for the two criteria $\frac{\chi_\tau}{\chi_\sigma}$ is around 130% (CLT1 and CLT2) for $f_0 = \frac{l}{200}$, as well as for $f_0 = \frac{l}{100}$ (the slenderness of the panel almost compensate for the default size). This difference is still significant, so that standard CLT panels under compression may fail due to rupture in the compressed layers rather than in the sheared layers. However, the safety margin is low and, may other shear forces be applied to the panel (such as wind forces for example), shear failure could be reached before axial failure. Having a shear strength criterion for easy verification of cross section seems thus a significant step forward for safer CLT walls design.

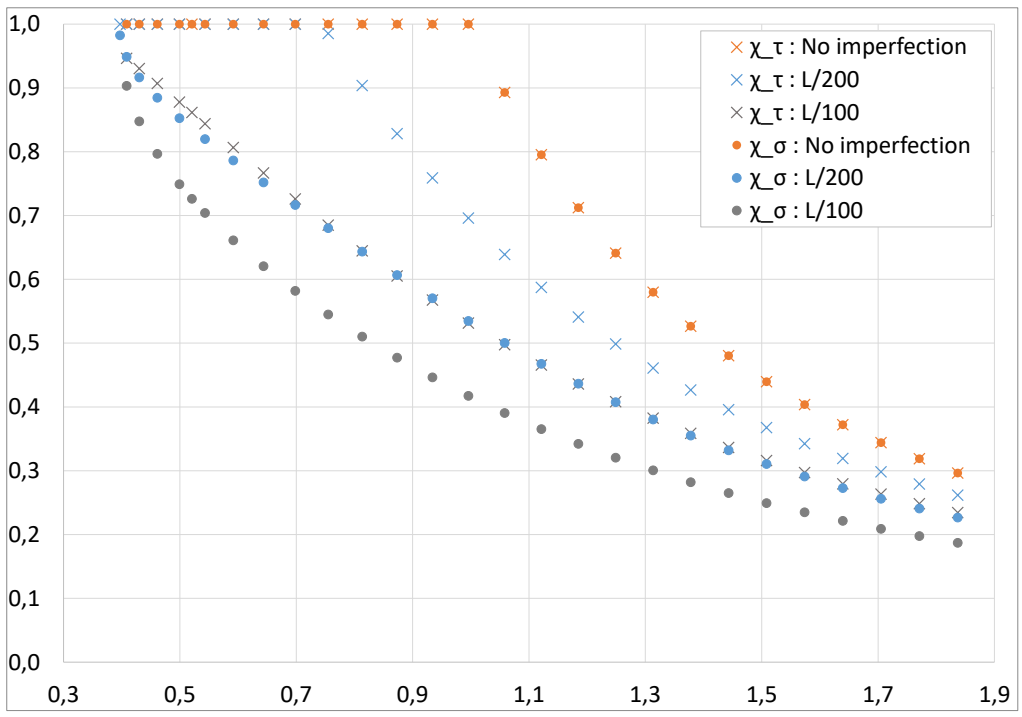

Figure 4: Comparison of short term bending and shear $\chi - \lambda$ criteria for CLT1.

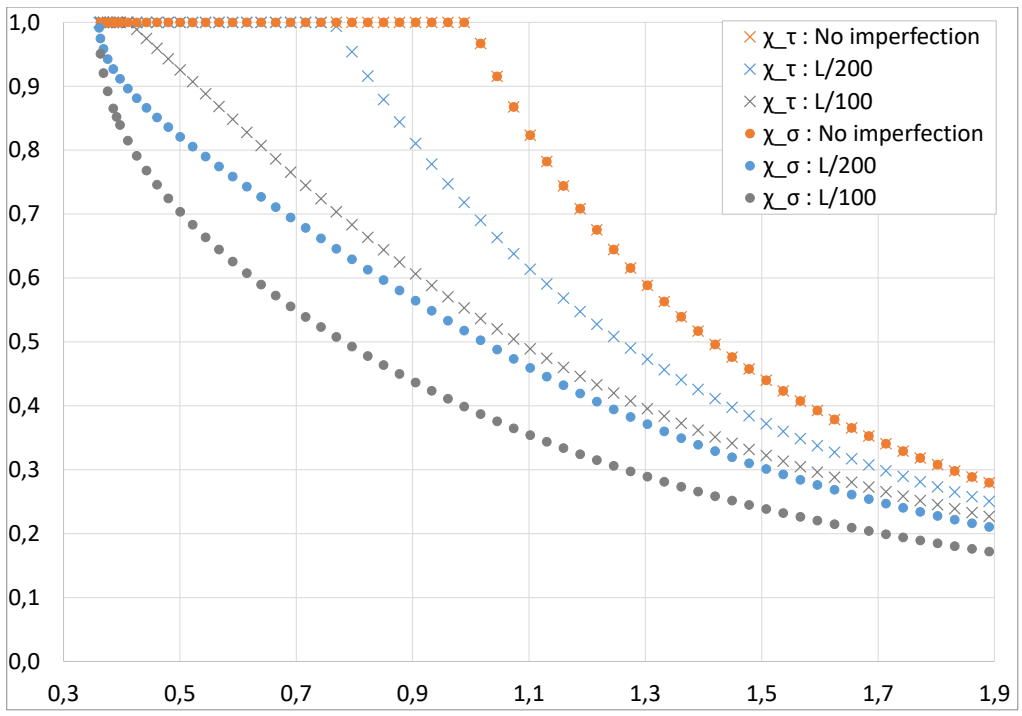

Figure 5: Comparison of short term bending and shear $\chi - \lambda$ criteria for CLT2.

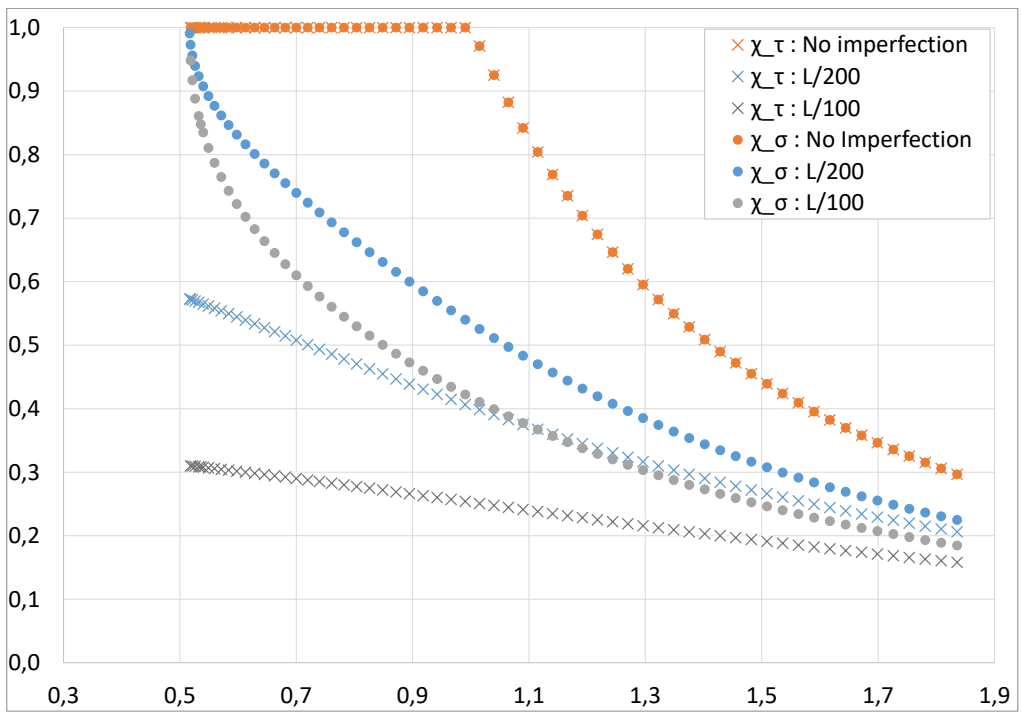

Figure 6: Comparison of short term bending and shear $\chi - \lambda$ criteria for CLT3.

4. Influence of creep on the critical load

In the previous section, the elastic behaviour of a column with initial imperfections under compression was investigated. Nevertheless, timber is a viscoelastic material and additional creep deformations must be added to these initial imperfections. In this section, the viscoelastic behavior of a timber column, studied by [1] among others, is recalled using the Euler beam model. It is then extended to a Timoshenko column with bending and shear creep. Finally, the influence of creep, particularly of shear creep, on the long term strength criterion is studied extending the early work of Becker and Rautenstrauch on creep-buckling for Euler beams [27, 28, 29] to Timoshenko beams.

4.1. Definition of the creep model

Several models have been suggested to account for the creep behavior of wood. Generally, models based on experiments lead infinite deflections at long-term [30]. However, models used in engineering practice assumed that the deflections are bounded, since for example, European standards, structures are designed for 50 years. A creep model that would provide finite deflection at long term and comply with actual wood model after 50 years will thus be a good candidate for estimating the long term stability of wooden structures. The simplest creep model which assumes long term finite deformations is the Poynting-Thomson model (Figure 7) composed of a linear elastic spring corresponding to elastic deformation and a Kelvin-Voigt model corresponding to creep deformation. Two elementary rheological models are used here:

- the linear spring which models an elastic material behaviour: $\sigma = E\varepsilon$
- the linear dash-pot which models a viscous material behaviour: $\sigma = \eta\frac{d\varepsilon}{dt}$ where t stands for time.

The differential equation corresponding to the Poynting-Thomson model (Figure 7) writes thus as:

$$\sigma + \frac{\eta_1}{E_0 + E_1}\frac{d\sigma}{dt} = \frac{E_0 E_1}{E_0 + E_1}\varepsilon + \frac{E_0\eta_1}{E_0 + E_1}\frac{d\varepsilon}{dt} \tag{33}$$

where σ and ε denote stress and strain in the studied direction. By noting $E_\infty = \frac{E_0 E_1}{E_0+E_1}$ as the long term stiffness and $t_E = \frac{\eta_1}{E_1}$ the characteristic time of the model, the differential equation (33) can be rewritten as:

$$\sigma + t_E\frac{E_\infty}{E_0}\frac{d\sigma}{dt} = E_\infty\varepsilon + t_E E_\infty\frac{d\varepsilon}{dt} \tag{34}$$

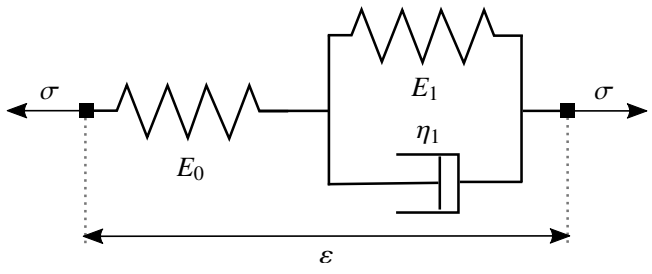

Figure 7: Poynting-Thomson creep model

For wood, the viscoelastic behavior of the nine components of the orthotropic elastic tensor should be considered individually. Nonetheless, their impact on CLT viscoelastic behaviour is complex because of the two levels of heterogeneities of CLT panels: at material scale and at layer scale. The viscoelastic behaviors of the various directions are indeed mixed in the global bending and shear behaviour of the CLT. Hence, in order to simplify the problem, we assume that the global bending and shear viscoelastic behaviours of the CLT are homogeneous and can be modeled by two independant Poynting-Thomson models replacing the local constitutive equations (5). The model characteristics are defined by $\overline{EI}_\infty$ the long term bending stiffness and $\overline{GS}_\infty$ the long term shear stiffness, and by t_σ and t_τ the characteristic time in bending and shear respectively:

$$\begin{cases} M + t_\sigma \dfrac{\overline{EI}_\infty}{\overline{EI}_0} \dfrac{dM}{dt} = \overline{EI}_\infty \varphi' + t_\sigma \overline{EI}_\infty \dfrac{d\varphi'}{dt} & \text{(35a)} \\ Q + t_\tau \dfrac{\overline{GS}_\infty}{\overline{GS}_0} \dfrac{dQ}{dt} = \overline{GS}_\infty \gamma + t_\tau \overline{GS}_\infty \dfrac{d\gamma}{dt} & \text{(35b)} \end{cases}$$

4.2. Long term buckling of a shear weak imperfect column

Assuming now classically that time and space variables can be separated, the solution of the previous differential system (35) are looked for with the following form:

$$\begin{cases} f(x,t) = f(t) \sin\left(\dfrac{\pi x}{l}\right) & \text{(36a)} \\ \gamma(x,t) = g(t) \cos\left(\dfrac{\pi x}{l}\right) & \text{(36b)} \end{cases}$$

where $f(t)$ and $g(t)$ are the mid-span deflection and the shear strain at support $x = 0$ at time t. By injecting these solutions into the constitutive equations (4) and then in the differential equations (35), a system of two differential equations of $f(t)$ and $g(t)$ only is obtained:

$$\begin{cases} t_\sigma \left(1 - \dfrac{P}{P_{E,0}}\right) \dfrac{df}{dt} + \left(1 - \dfrac{P}{P_{E,\infty}}\right) f - \dfrac{l}{\pi} \left(g - t_\sigma \dfrac{dg}{dt}\right) = f_0 & \text{(37a)} \\ t_\tau \dfrac{P}{\overline{GS}_0} \dfrac{df}{dt} + \dfrac{P}{\overline{GS}_\infty} f - \dfrac{l}{\pi} \left(g - t_\tau \dfrac{dg}{dt}\right) = 0 & \text{(37b)} \end{cases}$$

Introducing the generalised deflection vector $\underline{X}(t)$ as:

$$\underline{X}(t) = \begin{pmatrix} f(t) \\ \frac{l}{\pi} g(t) \end{pmatrix} \tag{38}$$

the problem (37) can be recast in:

$$\left(1 - \frac{P}{P_{\mathrm{cr},0}}\right) \frac{d\underline{X}}{dt}(t) + \underline{\underline{A}} \cdot \underline{X}(t) = \frac{f_0}{t_\sigma} \begin{pmatrix} 1 \\ \frac{P}{\overline{GS}_0} \end{pmatrix} \tag{39}$$

where

$$\underline{\underline{A}} = \begin{pmatrix} \frac{1}{t_\sigma}\left(1 - \frac{P}{P_{E,\infty}}\right) - \frac{1}{t_\tau}\frac{P}{\overline{GS}_\infty} & \frac{1}{t_\tau} - \frac{1}{t_\sigma} \\ \frac{1}{t_\sigma}\frac{P}{\overline{GS}_0}\left(1 - \frac{P}{P_{E,\infty}}\right) - \frac{1}{t_\tau}\frac{P}{\overline{GS}_\infty}\left(1 - \frac{P}{P_{E,0}}\right) & \frac{1}{t_\tau}\left(1 - \frac{P}{P_{E,0}}\right) - \frac{1}{t_\sigma}\frac{P}{\overline{GS}_0} \end{pmatrix} \tag{40}$$

The characteristic polynomial of the matrix $\underset{\sim}{\boldsymbol{A}}$ is given by:

$$\det\left(\underset{\sim}{\boldsymbol{A}} - \lambda \underset{\sim}{\boldsymbol{I}}\right) = \lambda^2 - b\lambda + c$$

where b and c are coefficients of the polynomial defined by:

$$b = \frac{1}{t_\sigma}\left(1 - \frac{P}{P_{\mathrm{cr},E,\infty}}\right) + \frac{1}{t_\tau}\left(1 - \frac{P}{P_{\mathrm{cr},G,\infty}}\right)$$

$$c = \frac{1}{t_\sigma t_\tau}\left(1 - \frac{P}{P_{\mathrm{cr},0}}\right)\left(1 - \frac{P}{P_{\mathrm{cr},\infty}}\right)$$

in which $P_{\mathrm{cr},E,\infty}$ and $P_{\mathrm{cr},G,\infty}$ are the long term critical buckling load when considering only the bending creep or the shear creep respectively:

$$\frac{1}{P_{\mathrm{cr},E,\infty}} = \frac{1}{P_{E,\infty}} + \frac{1}{\overline{GS}_0} \qquad \text{and} \qquad \frac{1}{P_{\mathrm{cr},G,\infty}} = \frac{1}{P_{E,0}} + \frac{1}{\overline{GS}_\infty}$$

$P_{\mathrm{cr},\infty}$ is the long term critical buckling load defined as:

$$\frac{1}{P_{\mathrm{cr},\infty}} = \frac{1}{P_{E,\infty}} + \frac{1}{\overline{GS}_\infty} \qquad \text{with} \qquad P_{E,\infty} = \frac{\pi^2 \overline{EI}_\infty}{l^2} \tag{41}$$

It is observed that the discriminant $\Delta = b^2 - 4c$ is always positive since it can be written as a sum of positive terms:

$$\Delta = \frac{1}{t_\sigma^2}\left(1 - \frac{P}{P_{\mathrm{cr},E,\infty}}\right)^2 + \frac{1}{t_\tau^2}\left(1 - \frac{P}{P_{\mathrm{cr},G,\infty}}\right)^2 + \frac{P^2}{t_\sigma t_\tau}\left(\frac{1}{\overline{GS}_\infty} - \frac{1}{\overline{GS}_0}\right)\left(\frac{1}{P_{E,\infty}} - \frac{1}{P_{E,0}}\right)$$

The two roots are thus real numbers. The solutions of equation (39) are then given by:

$$\underline{\boldsymbol{X}}(t) = \underline{\boldsymbol{X}}_1 \exp^{-\lambda_1 t} + \underline{\boldsymbol{X}}_2 \exp^{-\lambda_2 t} + \underline{\boldsymbol{X}}_\infty$$

where $\underline{\boldsymbol{X}}_1$ and $\underline{\boldsymbol{X}}_2$ are eigenvectors of $\underset{\sim}{\boldsymbol{A}}$ associated to roots λ_1 and λ_2 and $\underline{\boldsymbol{X}}_\infty$ is a constant vector corresponding to long term deflections.

$\underline{\boldsymbol{X}}(t)$ is finite at long term only if both roots λ_1 and λ_2 are positive. Therefore the column is stable at long term only if $b < 0$ and $c > 0$ which is equivalent to the following criteria:

$$\begin{cases} \dfrac{1}{P} > \dfrac{1}{t_\sigma + t_\tau}\left(\dfrac{t_\tau}{P_{\mathrm{cr},E,\infty}} + \dfrac{t_\sigma}{P_{\mathrm{cr},G,\infty}}\right) & \text{(42a)} \\ P < P_{\mathrm{cr},\infty} & \text{(42b)} \end{cases}$$

We note that, since $P_{\mathrm{cr},\infty} < P_{\mathrm{cr},E,\infty}$ and $P_{\mathrm{cr},\infty} < P_{\mathrm{cr},G,\infty}$, the criterion (42a) is always true given that the criterion (42b) is fulfilled. We thus keep only the second stability condition: $P < P_{\mathrm{cr},\infty}$.

Furthermore, we are here only interested in the long term deformation $\underline{\boldsymbol{X}}_{\infty}$. Provided that the stability criterion (42b) is fulfilled, long term deformation $\underline{\boldsymbol{X}}_{\infty}$ are derived from the equilibrium equation (39) by:

$$\underline{\boldsymbol{X}}_{\infty} = \begin{pmatrix} f_{\infty} \\ \frac{l}{\pi} g_{\infty} \end{pmatrix} = \frac{f_0}{1 - \frac{P}{P_{\mathrm{cr},\infty}}} \begin{pmatrix} 1 \\ \frac{P}{\overline{\overline{GS}}_{\infty}} \end{pmatrix} \tag{43}$$

Hence, the expression of the long term deflections of an imperfect beam f_{∞} (43) is similar to that of the short term deflection (20) and can be obtained by simply replacing the short term critical load $P_{\mathrm{cr},0}$ by the long term critical load $P_{\mathrm{cr},\infty}$ (41). As a consequence, the long term normal strength criterion can be adapted from the short term criterion (27) by replacing the short term buckling load $P_{\mathrm{cr},0}$ by the long term critical load $P_{\mathrm{cr},\infty}$ and considering long term elastic characteristics following the same approach :

$$\frac{P}{P_{u,\infty}} < \frac{2}{\left(1 + \omega_{\infty} + \bar{\lambda}_{\infty}^2\right) + \sqrt{\left(1 + \omega_{\infty} + \bar{\lambda}_{\infty}^2\right)^2 - 4\bar{\lambda}_{\infty}^2}} = \chi_{\sigma,\infty} \tag{44}$$

with:

$$P_{u,\infty} = \sigma_{u,\infty} \frac{ES_{\infty}}{E_{L,\infty}} \quad \text{and} \quad \omega_{\infty} = \frac{ES_{\infty} h f_0}{2\overline{EI}_{\infty}} \quad \text{and} \quad \bar{\lambda}_{\infty} = \sqrt{\frac{P_{u,\infty}}{P_{\mathrm{cr},\infty}}} \tag{45}$$

Following the same reasonning, the expression of the long term shear strain g_{∞} (43) is also similar to that of the short term shear strain (22a). The shear strength criterion in the cross-layer can thus be derived from the short term criterion (32) by replacing the critical buckling load and the shear stiffness by their long term values:

$$\frac{P}{P_{u,\infty}} < \frac{1}{\frac{\pi f_0}{l} \frac{P_{u,\infty}}{Q_{u,\infty}} + \bar{\lambda}_{\infty}^2} = \chi_{\tau,\infty} \tag{46}$$

with:

$$Q_{u,\infty} = \tau_{u,\infty} \frac{\overline{EI}_{\infty}}{\int_0^{\frac{h}{2}} E_{\infty}(z) z dz} \tag{47}$$

Two long term strength criteria, one for normal stresses in longitudinal layers, one for shear stresses in cross layers, have thus been developped. They will be compared in a similar way to the short term criteria (see Section 3.4) in the following section. It is worth highlighting that in both criteria, the critical load involved in the calculation of the modified slenderness is based on the long term characteristics, contrary to actual standards which base the calculation of the critical load on short term material characteristics. The Standards are hence conservative, but they could be made more precise adjusting the reduced slenderness with the duration of the load.

4.3. Influence of the orthotropic creep on the strength criteria

To investigate the influence of the viscoelastic characteristics of CLT, we build on the normalised approach of European Standards for the evaluation of long term material characteristics. Long

term properties are hence defined by using two creep factors: k_{def} for the stiffness and k_{mod} for the strength, so that:

$$\begin{cases} E_\infty = \dfrac{E_0}{1+k_{\text{def}}} & \text{(48a)} \\ \sigma_{u,\infty} = k_{\text{mod}}\sigma_u & \text{(48b)} \end{cases}$$

Today, there are no specification for k_{def} and k_{mod} for CLT in EC5, but the pre-norm found by the authors recommands to use the same value as for plywood. For a class 2 panel under permanent compression, this corresponds to $k_{\text{mod}} = 0.6$ and $k_{\text{def}} = 1$. This is however a subject that is still under active discussion, especially because, to the authors knowledge, there are no experimental data on the evolution with time of the equivalent cross layer rolling-shear strength (only at grain scale [15] or some). At the panel scale, Nakajima [31] and Pirvu [18] observed that the variation of the bending strength of CLT with time is very similar to what is observed for solid timber. This is contradictory with the experimentsof Li and Lam based on damage cumulation for fatigue [32], which demonstrated that k_{mod} might fall to 0.4 for CLT [14].

These last observation go well along with those concerning the reduction factor of stiffnesses. Indeed the experiments cited in the introduction [15, 16, 17, 18] suggest that the sheared cross-layers in CLT creep faster than the compressed longitudinal layers. Quantitatively, it is however difficult to conclude on how quicker cross layers creep. Based on the literature, it seems reasonnable (but somehow optimistic) to assume that shear creep is twice larger than bending creep: $k_{\text{def},\tau} = 2k_{\text{def},\sigma}$ where $k_{\text{def},\sigma}$ and $k_{\text{def},\tau}$ are the bending creep factor and the shear creep factor respectively.

So, assuming in the same way, that there is a different modification factor for strength, one for bending $k_{\text{mod},\sigma} = 0.6$ and one for shear $k_{\text{mod},\tau} = 0.4$, which take value according to Li and Lam [14], we find a quite consistent set of material variable where strength and stiffness damage are proportionnel:

$$\frac{1+k_{\text{def},\tau}}{1+k_{\text{def},\sigma}} = \frac{k_{\text{mod},\sigma}}{k_{\text{mod},\tau}} = 1.5 \tag{49}$$

The long term critical buckling load $P_{\text{cr},\infty}$ (41), long term axial strength $P_{u,\infty}$ (45) and long term shear strength $Q_{u,\infty}$ (47) could thus be estimated from the short term characteristics by:

$$\begin{cases} \dfrac{1}{P_{\text{cr},\infty}} = \dfrac{1+k_{\text{def},\sigma}}{P_{E,0}} + \dfrac{1+k_{\text{def},\tau}}{\overline{GS}_0} & \text{(50a)} \\ P_{u,\infty} = k_{\text{mod},\sigma}P_{u,0} \quad \text{and} \quad Q_{u,\infty} = k_{\text{mod},\tau}Q_{u,0} & \text{(50b)} \end{cases}$$

The corresponding χ/λ curves are plotted in Figures 8, 9 and 10 for the three configurations. For indication, modified slenderness at long term are given for usual height of CLT panels in Table 5 (one can see that they do not differ much from the short terms values given in Table 4).

For CLT3, the aerated panel, like at short term, the shear criterion always dominates. For the other two configurations however (CLT1 and CLT2), for standard imperfection size ($f_0/l = 1/200$), the long term normal criterion still dominates the shear criterion but the ratio between both criteria is lowered (see Table 6). For a double size imperfection on the contrary ($f_0/l = 1/100$), the shear criterion now dominates for low slenderness, which means for $l < 2.3\,\text{m}$ for CLT1 and $l < 3.3\,\text{m}$ for CLT2 which is typically the range of a wall height in buildings.

h	CLT1	CLT2	CLT3
3 m	1.08	0.61	0.73
6 m	2.00	0.97	1.02

Table 5: Order of magnitude of the modified slenderness $\bar{\lambda}$ at short term for the three reference configurations.

χ_σ/χ_τ	CLT1	CLT2	CLT3
Short term	130%	178%	67%
Long term	113%	133%	48%

Table 6: Comparison of short and long term values of χ_σ/χ_τ for standard imperfection $f_0/l = 1/200$.

Considering finally that the shear stresses accounted here are only due to second order effects of normal stresses and that there are generally other sources of shears stresses in walls, it seems a necessity for the authors to introduce a criterion for shear stresses along with the criterion for normal stresses when buckling is considered. This holds for short term and long term verifications.

Moreover, it must be added here that the shear force is maximum at the support where a lot of local stress concentrations occur due to connection which are the wellknown weak point of wooden construction. The influence of the shear forces induced by buckling on the design of connection is for sure a topic to be developped in future research.

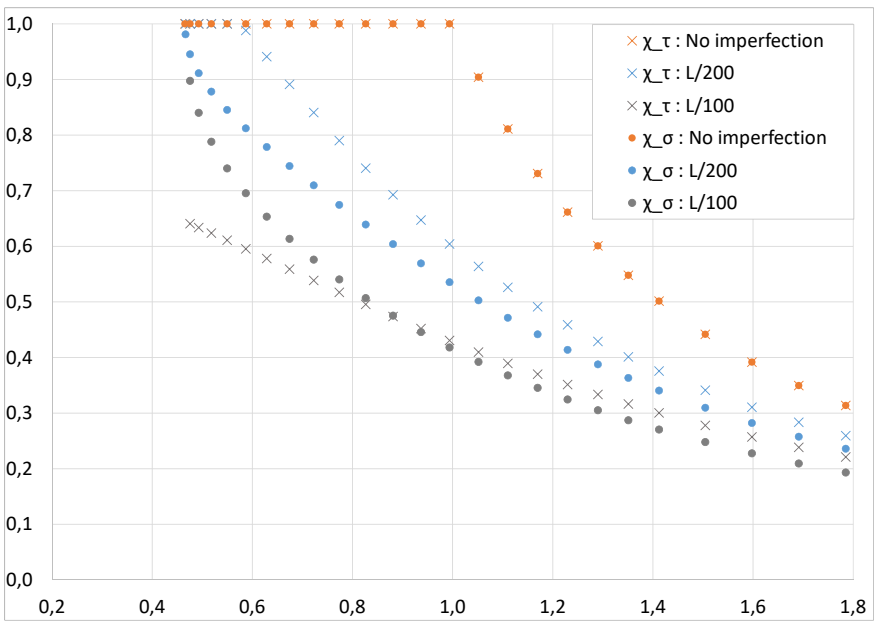

Figure 8: Normal and shear $\chi - \lambda$ criteria at long-term for CLT1.

5. Conclusion

In this paper, the Ayrton-Perry approach was adapted for a CLT wall under compression and a similar shear criterion was introduced. It was observed that the shear criterion can be relevant for thick walls and for CLT with a low cross-layer shear strength and in a less critical way, a low cross-layer shear stiffness. This criterion was then extended to the long term stability of CLT panels introducing timber viscoelastic behaviour. Some practical configurations have been investigated assuming that creep in the rolling shear direction was twice higher than in the longitudinal direction.

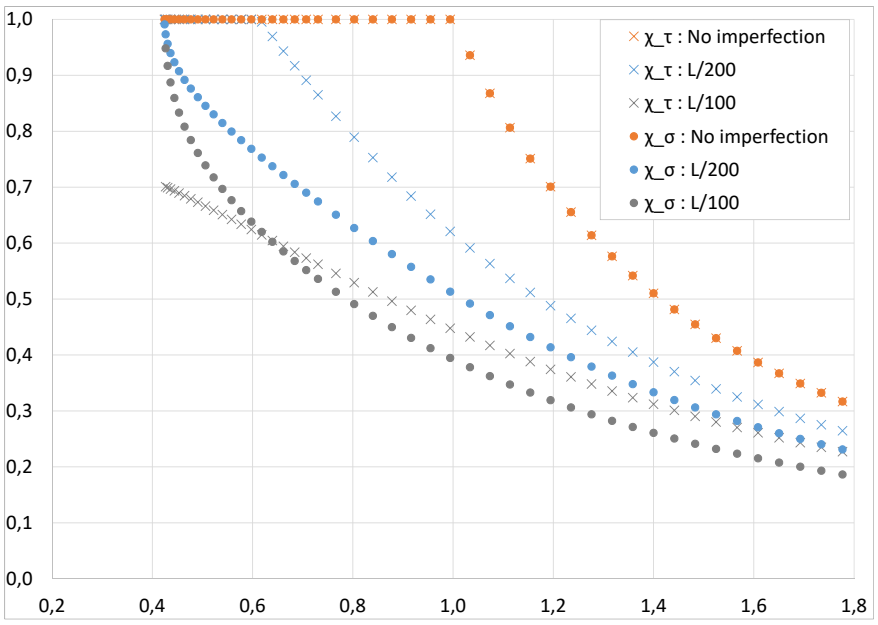

Figure 9: Normal and shear $\chi - \lambda$ criteria at long-term for CLT2.

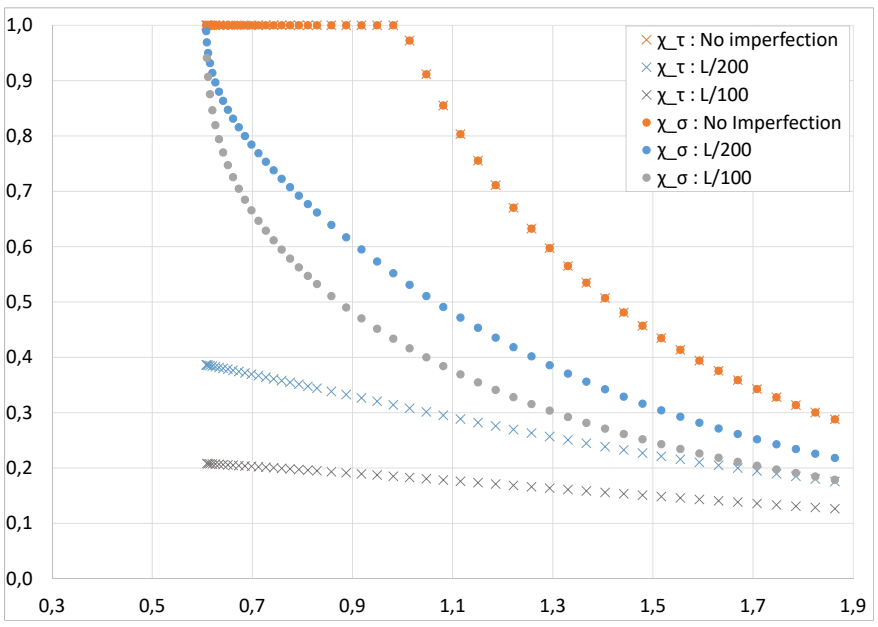

Figure 10: Normal and shear $\chi - \lambda$ criteria at long-term for CLT3.

It was observed that, in this case, the safety margin was significantly reduced and that with double size imperfections, shear failure might occur before compression failure.

These conclusions on the buckling of CLT panels go in the same direction as previous work on bending of CLT panels: the introduction of a systematic shear verification in cross layers seems necessary for safe design with CLT. To this end, further investigation of the evolution of the rolling shear strength and stiffness over time seems necessary and would be very helpfull for the development of CLT panels in high rise building where compression forces are high.

Finally, it is worth pointing out that, in the case of buckling, shear forces are maximum at the supports, where it is well known that according to Saint Venant principle, the beam models fail to predict accurately the stress field. Indeed, at the supports, the stress field is generally three dimensionnal and directly linked with the way forces are applied and with the technological solution retained for the connection. Hence, the proposed criterion could be seen as a simple way of estimating the risk of shear failure for practionners; an accurate estimation of the failure load would need a refined local analysis of the connection system that would take into account second order effects linked with compression load and buckling.

References

[1] Z. Bažant, L. Cedolin, Stability of structures, ASME Appl. Mech. Rev. (1991).

[2] K. Kalochairetis, C. Gantes, Numerical and analytical investigation of collapse loads of laced built-up columns, Computers and Structures 89 (11-12) (2011) 1166–1176. doi:10.1016/j.compstruc.2010.10.018.

[3] K. Kalochairetis, C. Gantes, Elastic buckling load of multi-story frames consisting of timoshenko members, Journal of Constructional Steel Research 71 (2012) 231–244. doi:10.1016/j.jcsr.2011.11.007.

[4] Y. Frostig, Buckling of sandwich panels with a flexible core, high-order theory, International Journal of Solids and Structures 35 (3) (1998) 183 – 204. doi:https://doi.org/10.1016/S0020-7683(97)00078-4.

[5] J. Moita, A. Araújo, V. Franco Correia, C. Mota Soares, C. Mota Soares, Buckling and geometrically nonlinear analysis of sandwich structures, International Journal of Mechanical Sciences 92 (2015) 154–161. doi:10.1016/j.ijmecsci.2014.12.008.

[6] R. Yeghnem, H. Z. Guerroudj, L. H. H. Amar, S. A. Mefta, S. Benyoucef, A. Tounsi, E. A. A. Bedia, Numerical modeling of the aging effects of rc shear walls strengthened by cfrp plates: A comparison of results from different code type models, Computers and Concrete 19 (5) (2017) 579–588. doi:https://doi.org/10.12989/cac.2017.19.5.579.

[7] A. Thiel, ULS and SLS design of CLT and its implementation in the CLTdesigner, in: Focus solid timber solutions—European conference on cross laminated timber (CLT). The University of Bath, Bath, 2013.

[8] O. Perret, A. Lebée, C. Douthe, K. Sab, The bending–gradient theory for the linear buckling of thick plates: Application to cross laminated timber panels, International Journal of Solids and Structures 87 (2016) 139–152.

[9] E. C. for Standardisation, Eurocode 5 - design of timber structures (1993).

[10] E. Karacabeyli, B. Douglas, CLT Handbook: cross-laminated timber, FPInnovations, 2013.

[11] C. Stora Enso, Document technique d'application 3/13-750 : Panneaux bois a usage structurel, European Technical Agreement (2014).

[12] W. Ayrton, J. Perry, On struts, The engineer 62 (1886) 464.

[13] A. Thiel, H. Krenn, Buckling lods for cross-laminated timber elements under uniaxial in-plane compression, in: Proceedings of the 14th World Conference on Timber Engineering (WCTE 2016), Vienna, 2016.

[14] Y. Li, F. Lam, Reliability analysis and duration-of-load strength adjustment factor of the rolling shear strength of cross laminated timber, Journal of Wood Science 62 (6) (2016) 492–502. doi:10.1007/s10086-016-1577-0.

[15] A. Schniewind, J. Barrett, Wood as a linear orthotropic viscoelastic material, Wood Science and Technology 6 (1) (1972) 43–57.

[16] R. Jöbstl, G. Schickhofer, Comparative examination of creep of GLT – and CLT – slabs inbending, in: International Council for Research and Innovation in builduing and construction, 2007.
[17] F. Colling, Creep behavior of cross laminated timber in service class 2, Tech. rep., Hochschule Augsburg, University of Applied Sciences (2014).
[18] C. Pirvu, E. Karacabeyli, Time-dependent behaviour of CLT, in: World Conference on Timber Engineering, 2014.
[19] O. Perret, A. Lebée, C. Douthe, K. Sab, Experimental determination of the equivalent-layer shear stiffness of CLT through four-point bending of sandwich beams, Construction and Building Materials 186 (2018) 1132–1143. doi:10.1016/j.conbuildmat.2018.07.102.
[20] T. Ehrhart, R. Brandner, Rolling shear: Test configurations and properties of some european soft- and hardwood species, Engineering Structures 172 (2018) 554–572. doi:10.1016/j.engstruct.2018.05.118.
[21] R. Brandner, G. Flatscher, A. Ringhofer, G. Schickhofer, A. Thiel, Cross laminated timber (CLT): overview and development, European Journal of Wood and Wood Products 74 (3) (2016) 331–351. doi:10.1007/s00107-015-0999-5.
[22] G. Schickhofer, R. Brandner, H. Bauer, Introduction to CLT, product properties, strength classes, of COST Actions FP1402 & FP1404 KTH Building Materials, 10.3. 2016 Cross Laminated Timber–A competitive wood product for visionary and fire safe buildings (2016) 9.
[23] O. Perret, C. Douthe, A. Lebée, K. Sab, Equivalent stiffness of timber used in CLT - closed-form estimates and numerical validation, European Journal of Wood and Wood Products 3 (2019).
[24] L. Franzoni, A. Lebée, F. Lyon, G. Forêt, Elastic behavior of cross laminated timber and timber panels with regular gaps: Thick-plate modeling and experimental validation, Engineering Structures 141 (2017) 402–416.
[25] L. Franzoni, A. Lebée, F. Lyon, G. Forêt, Closed-form solutions for predicting the thick elastic plate behavior of CLT and timber panels with gaps, Engineering Structures 164 (2018) 290–304. doi:10.1016/j.engstruct.2018.02.073.
[26] P. Mayencourt, C. Mueller, Structural optimization of cross-laminated timber panels in one-way bending, Structures (2018). doi:https://doi.org/10.1016/j.istruc.2018.12.009.
[27] P. Becker, K. Rautenstrauch, Deformation and stability of columns of visco elastic material wood, in: Proceedings of the CIBW18 Meeting. Savonlinna, Vol. 31, 1998.
[28] P. Becker, K. Rautenstrauch, Time-dependent material behavior applied to timber columns under combined loading. part ii: Creep-buckling, European Journal of Wood and Wood Products 59 (6) (2001) 491–495.
[29] P. Becker, K. Rautenstrauch, Time-dependent material behavior applied to timber columns under combined loading. part i: Creep deformation, European Journal of Wood and Wood Products 59 (5) (2001) 380–386.
[30] P. Gressel, Prediction of long-term deformation-behavior from short-term creep experiments, Holz Als Roh-und Werkstoff 42 (8) (1984) 293–301.
[31] N. Shiro, M. Atsushi, S. Tatsuya, A. Yasuhiro, Y. Nobuyoshi, H. Takeshi, A. Naoto, Y. Motoi, Creep and duration of load characteristics of cross laminated timber, in: Proceedings of the 13th World Conference on Timber Engineering (WCTE 2014), Quebec City, 2014.
[32] Y. Li, F. Lam, Low cycle fatigue tests and damage accumulation models on the rolling shear strength of cross-laminated timber, Journal of Wood Science 62 (3) (2016) 251–262. doi:10.1007/s10086-016-1547-6.